Learning the CSI Recovery in FDD Systems

Wolfgang Utschick, *Fellow*, IEEE, Valentina Rizzello, *Student Member, IEEE,*

Michael Joham, *Member, IEEE,*

Zhengxiang Ma, *Member, IEEE,* and Leonard Piazzi, *Member, IEEE*

Abstract

We propose an innovative machine learning-based technique to address the problem of channel acquisition at the base station in frequency division duplex systems. In this context, the base station reconstructs the full channel state information in the downlink frequency range based on limited downlink channel state information feedback from the mobile terminal. The channel state information recovery is based on a convolutional neural network which is trained exclusively on collected channel state samples acquired in the uplink frequency domain. No acquisition of training samples in the downlink frequency range is required at all. Finally, after a detailed presentation and analysis of the proposed technique and its performance, the "transfer learning" assumption of the convolutional neural network that is central to the proposed approach is validated with an analysis based on the maximum mean discrepancy metric.

Index Terms

Machine learning, massive MIMO, FDD systems, transfer learning, maximum mean discrepancy, convolutional neural networks, deep learning.

I. INTRODUCTION

THE massive multiple-input multiple-output (MIMO) technology is one of the most prominent directions to scale up capacity and throughput in modern communication systems [1]. In particular, the multi-antennas support at the base station (BS) makes simple techniques such as spatial multiplexing and beamforming very efficient regarding the spectrum or the bandwidth

W. Utschick, V. Rizzello and M. Joham are with the Professur für Methoden der Signalverarbeitung, Technische Universität München, Munich, 80333, Germany. {utschick, valentina.rizzello, joham}@tum.de

Z. Ma and L. Piazzi are with Futurewei Technologies, at 400 Crossing Blvd., Bridgewater, New Jersey 08807, USA. {zma@futurewei.com, lpiazzi@verizon.net}

utilization. However, to take full advantage of Massive MIMO systems, the base station must have the best possible channel estimation. Considering the typically stringent delay requirements in wireless mobile communication systems, the channel state information (CSI) has to be acquired in very short regular time intervals.

A variety of solution approaches developed for this purpose are based on time division duplex (TDD) mode. TDD means that both the BS and the mobile terminal (MT) share the same bandwidth, but the BS and the MT cannot transmit in the same time interval. Due to the fact that they both share the same bandwidth, the uplink (UL) and downlink (DL) channels are reciprocal, i.e., once the BS estimates the UL channel, it also knows the DL channel without any additional feedback overhead [2].

On the other hand, in frequency division duplex (FDD) mode, the BS and the MT transmit in the same time slot but at different frequencies. This breaks the reciprocity between UL CSI and DL CSI and makes it hard for the network operators with FDD licenses to obtain an accurate DL CSI estimate for transmit signal processing [3]. The usual solution to the problem is to either extrapolate the DL CSI from the estimate of the UL CSI at the BS, or to transfer the DL CSI estimated at the MT to the BS directly or in a highly compressed version.[1] The former rely on available system models and aim to rather estimate the second-order information of the DL channel, namely the covariance matrix of the DL CSI, which is supposed to stay constant for several coherence intervals. See [4] for latest results in this direction and [5] for a reference to a very early attempt by the author. In contrast, data-driven approaches do not make assumptions about the underlying channel model, but instead use paired training samples of UL CSI and DL CSI along with a machine learning procedure that predicts the DL CSI considering the UL CSI as input [6]–[11]. In the end, the most common solutions encountered in practice are based on feedback-based methods. In addition to a plethora of classical approaches, cf. [12], a promising variant that has recently been proposed several times in different versions is to elegantly combine the learning of a sparse feedback format with the task of performing channel reconstruction at the BS using an autoencoder neural network [13]–[18]. To this end, these approaches rely on implementing the encoder and decoder part of the jointly trained autoencoder distributed on MT and the BS, i.e., whereas the encoder unit at the MT maps channel estimates

[1]Another common solution is to omit the feedback of the CSI and to signal only channel quality indicators of the transmission properties.

or corresponding observations of pilot data to an appropriate feedback format, the decoder unit at the BS reconstructs the complete DL channel estimates based on the received feedback. The approach in [19] instead proposes a centralized training at the BS station based on DL CSI data, where the DL CSI is compressed at the user side using a Gaussian random matrix and it is then fed back at the BS which reconstructs it with a neural network. In [20] a model-based neural network has been trained to jointly design the pilot pattern and estimate the DL CSI in FDD MIMO orthogonal frequency division multiplex systems (OFDM).

The approach proposed in this paper also belongs to the data-driven category. However, compared to other approaches found in the literature, we consider that in real-world systems (i) the implementation of a distributed training setup between BS and MT is rather challenging in practice, (ii) a centralized UL-DL CSI based supervised training would require a large number of true UL-DL CSI *pairs*, which are very costly to obtain at the same location - usually the BS, (iii) and thus a centralized training at the BS using true DL CSI data would impose an unrealistic overhead, as transporting the data is particularly inefficient since it leads to excessive network usage. With our contribution:

1) the practical issue of "DL CSI data acquisition" by training a neural network at the BS in a "centralized fashion" using only UL CSI data available at the BS is addressed;

2) the typical overhead of the "federated" learning framework, where the MT would have to send the gradients to the BS several times during training to update the neural network parameters, is avoided;

3) a new perspective to FDD systems is presented, where we show that the BS can obtain the DL CSI estimate with a learning which is solely based on UL CSI data;

4) a justification of the proposed "UL-DL conjecture" using the maximum-mean-discrepancy metric is given;

5) and a neural network approach which consists on convolutional layers to show that the proposed "UL-DL conjecture" works is presented. Please keep in mind that the neural network architecture we used, which we kept as simple as possible, is only a means to show that our idea works in general. Despite the already promising performance, further optimizations of the architecture are the subject of future research.

In the following, we present the principle of the training based solely on UL CSI. By denoting H_{UL} and $H_{\mathrm{DL}} \in \mathbb{C}^{N_a \times N_c}$ as the true uplink and downlink channel matrices, respectively, where
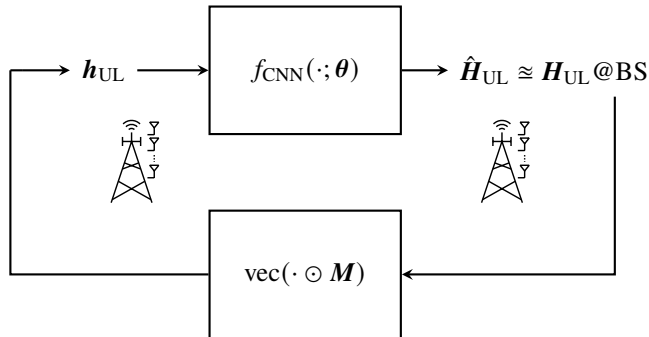
Figure 1. CNN training based on paired UL CSI $(\boldsymbol{h}_{\mathrm{UL}}, \boldsymbol{H}_{\mathrm{UL}})$ collected at the BS.
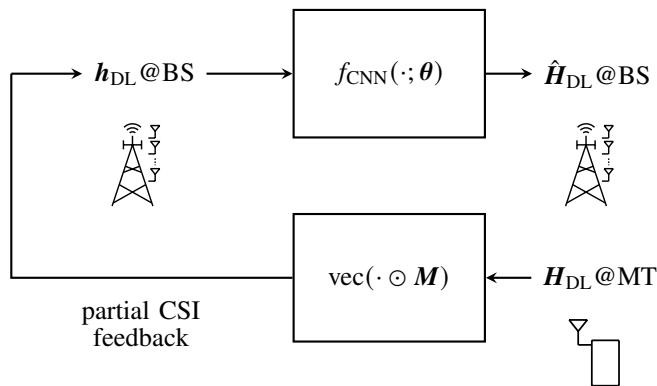
Figure 2. DL CSI recovery based on partial DL CSI from MT.

N_{a} and N_{c} denote the number of antennas at the BS and the number of subcarriers, respectively, we can summarize our approach in two stages.

Firstly, we train a convolutional neural network (CNN) at the BS to reconstruct the full UL channel matrix from a low-sampled version of itself, cf. Figure 1. This stage can be formulated as

$$\hat{\boldsymbol{H}}_{\mathrm{UL}} = f_{\mathrm{CNN}}(\boldsymbol{h}_{\mathrm{UL}}; \boldsymbol{\theta}), \tag{1}$$

where $\hat{\boldsymbol{H}}_{\mathrm{UL}} \in \mathbb{C}^{N_{\mathrm{a}} \times N_{\mathrm{c}}}$ denotes the reconstructed UL CSI, $f_{\mathrm{CNN}}(\cdot; \boldsymbol{\theta})$ denotes the function instantiated by the CNN, and $\boldsymbol{h}_{\mathrm{UL}}$ represents the low-sampled version of the true UL channel matrix. Note that the training phase of the CNN at the BS is solely based on collected CSI estimates in the UL frequency range.

In the second stage, we assume that the MT, which has access to the full DL channel matrix,[2]

feeds the low-sampled version of it back to the BS, where this represents the required input of the trained CNN at the BS in order to reconstruct the full DL channel matrix, cf. Figure 2. We can summarize this stage as

$$\hat{\boldsymbol{H}}_{\mathrm{DL}} = f_{\mathrm{CNN}}(\boldsymbol{h}_{\mathrm{DL}}; \boldsymbol{\theta}), \tag{2}$$

where $\hat{\boldsymbol{H}}_{\mathrm{DL}} \in \mathbb{C}^{N_a \times N_c}$ denotes the reconstructed DL channel matrix, as in (1), $f_{\mathrm{CNN}}(\cdot; \boldsymbol{\theta})$ still denotes the function instantiated by the UL-trained CNN, and $\boldsymbol{h}_{\mathrm{DL}}$ contains the low-sampled version of the true DL channel matrix with the same format and size as in the first stage.

The proposed technique is obviously based on the conjecture that learning the reconstruction in the UL domain can be "transfered" over the frequency gap between UL and DL center frequencies to the DL domain without any further adaptation.

The rest of the paper is organized as follows. First, in Section II, we describe how the channel dataset is constructed. Then, in Section III, we present the details of the UL training procedure, while in Section IV, we deal with the reconstruction of the DL CSI. The obtained results are discussed in Section V. In Section VI, we evaluate how the learned CNN performs on another cell. Finally, in Section VII with an analysis based on the maximum mean discrepancy (MMD) metric, we justify the stated conjecture and its results from a statistical point of view.

II. SCENARIO AND DATASET DESCRIPTION

The following study is based on an FDD system that utilizes center frequencies below 6 GHz and we explore three different frequency gaps between UL and DL, namely 120 MHz, 240 MHz, and 480 MHz. The channel state information for the UL and DL scenario has been generated with the MATLAB based channel simulator QuaDRiGa version 2.2 [21], [22].

We simulate an urban microcell (UMi) non-line-of-sight (NLoS) scenario, where the number of multi-path components (MPCs) is $L = 58$. The BS is placed at a height of 10 meters and is equipped with a uniform planar array (UPA) with $N_a = 8 \times 8$ "3GPP-3d" antennas, while the users have a single omni-directional antenna each. Additionally, the BS antennas are tilted by 6 degrees towards the ground to point in the direction of the users.

---

[2]Without any restriction on the principle, it would also be conceivable that the channel estimation in the MT is limited only to the part of the full DL channel matrix that is considered for feedback.

We consider a bandwidth of approximately 8 MHz divided over $N_c = 160$ subcarriers. The UL center frequency is 2.5 GHz while the DL center frequencies are 2.62 GHz, 2.74 GHz, and 2.98 GHz. The radio propagation characteristic of the entire cell which supports a radius of 150 m has been uniformly sampled at 3×10^5 different locations and for each sample, the channels at the predefined frequency ranges are collected. Consequently, the dataset is split into three groups of $2, 4 \times 10^5$, 3×10^4 and 3×10^4 samples, where each sample consists of the four matrices $\boldsymbol{H}_{\text{UL}}$, $\boldsymbol{H}_{\text{DL-120}}$, $\boldsymbol{H}_{\text{DL-240}}$ and $\boldsymbol{H}_{\text{DL-480}} \in \mathbb{C}^{N_a \times N_c}$. Note that since our training is based on the UL CSI exclusively, only the test set of the three DL CSI datasets (`DL@120...480`) will be used.

In order to maintain the spatial consistency of the scenario, for a given environment, the following parameters are identical in UL and DL domain: positions of BS and MTs, propagation delays and angles for each MPC, and large scale fading parameters. Small scale parameters are chosen independently, consistent with the stochastic nature of phase shifts associated with MPCs as frequency changes, due to which exptrapolations over the UL-DL frequency gap are hardly possible. Here, the proposed solution approach based on mere reconstruction in the same bandwidth proves to be particularly advantageous.

Within QuaDRiGa, the channel between the N_a transmit antennas and the single receive antenna at the MS is modeled as

$$[\boldsymbol{H}]_n = \sum_{\ell=1}^{L} \boldsymbol{g}_\ell \exp(-j2\pi f_n \tau_\ell),$$

corresponding to the n-th column vector of the introduced channel matrix. The parameters are the n-th carrier frequency f_n of N_c carriers, the time delay τ_ℓ of the ℓ-th of a total of L paths and $\boldsymbol{g}_\ell$ as the channel vector consisting of the complex-valued channel gains $g_{k,\ell}$ of the ℓ-th path between the k-th transmit antenna and the receive antenna at the MS, depending on the polarimetric antenna responses at the receiver and the transmitter and on the arrival and departure angles $(\phi_\ell^a, \theta_\ell^a)$ and $(\phi_\ell^d, \theta_\ell^d)$.[3]

The dataset is normalized according to

$$\boldsymbol{H} \leftarrow 10^{-\text{PG}_{\text{dB}}/20} \boldsymbol{H} \tag{3}$$

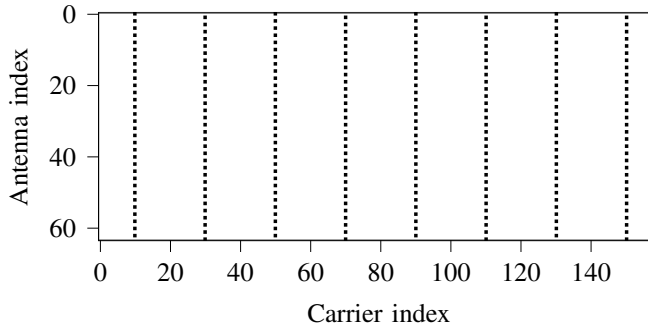[3] Azimuthal and elevation angles with respect to the array geometry under consideration.

Figure 3. Example of binary mask with $\eta = 0,025$, where the black squares represent elements with value 1.

where PG_{dB} is the path gain in decibels. Note that the information of the PG for each individual sample is contained in the channel object generated with QuaDRiGa. Therefore, no further computation is required.

III. LEARNING IN THE UPLINK DOMAIN

In this section, the details of the training procedure are presented. As outlined in Section I, we follow the conjecture that the reconstruction of the DL CSI based on a small portion of feedback information can be learned in the UL domain without any requirement of training data in the DL domain. Consequently, the training can be carried out entirely at the BS utilizing the UL CSI which is directly collected at the BS without any feedback requirements. Specifically, the UL channel matrix $\boldsymbol{H}_{UL} \in \mathbb{C}^{N_a \times N_c}$ is transformed into $\boldsymbol{H}_{UL}^{real} \in \mathbb{R}^{N_a \times N_c \times 2}$ by stacking the real and imaginary parts along the third dimension of a tensor. Thanks to this transformation, we work only with real-valued numbers. In the next step, the UL channel matrix $\boldsymbol{H}_{UL}^{real}$ is downsampled to

$$\boldsymbol{h}_{UL} = \text{vec}(\boldsymbol{H}_{UL}^{real} \odot \boldsymbol{M}) \tag{4}$$

where $\odot \boldsymbol{M}$ represents a binary masking that only keeps a reduced amount of totally $2\eta N_a N_c$ real-valued entries of the channel matrix $\boldsymbol{H}_{UL}^{real}$ with $0 < \eta \ll 1$, i.e., the compression ratio corresponding to the binary masking is given by $1/\eta$. In addition, $\text{vec}(\cdot)$ denotes the vectorization operation. The matrix $\boldsymbol{M}$ is designed such that we just select out $2\eta N_c$ of all carriers and for each carrier we consider only half (every second) of the antennas coefficients. Moreover, the selected carriers are equidistantly spaced in the carrier domain. These choices of parameters

Table I

PROPOSED CNN ARCHITECTURE.

Layer type	Output shape	#Parameters θ
Input	512	0
Reshape using mask	$64 \times 160 \times 2$	0
Conv2D transposed, dilation=15	$64 \times 160 \times 32$	608
Batch normalization	$64 \times 160 \times 32$	128
ReLU	$64 \times 160 \times 32$	0
Conv2D transposed, dilation=7	$64 \times 160 \times 64$	18496
Batch normalization	$64 \times 160 \times 64$	256
ReLU	$64 \times 160 \times 64$	0
Conv2D transposed, dilation=4	$64 \times 160 \times 128$	73856
Batch normalization	$64 \times 160 \times 128$	512
ReLU	$64 \times 160 \times 128$	0
Conv2D transposed, dilation=2	$64 \times 160 \times 64$	73792
Batch normalization	$64 \times 160 \times 64$	256
ReLU	$64 \times 160 \times 64$	0
Conv2D transposed, dilation=2	$64 \times 160 \times 32$	18464
Batch normalization	$64 \times 160 \times 32$	128
ReLU	$64 \times 160 \times 32$	0
Conv2D transposed	$64 \times 160 \times 2$	578
Multiplication (with reversed mask)	$64 \times 160 \times 2$	0
Addition (with Input)	$64 \times 160 \times 2$	0

are made with regard to the typically small size of affordable feedback information in the DL domain when analyzing the FDD system.

An example mask with $\eta = 0.025$ and thus a compression ratio of 40 is illustrated in Figure 3, where 8 out of 160 carriers are considered, and for each carrier, 32 out of 64 antenna coefficients are selected. In order to attract the readers' attention to the method rather than to the optimization of the mask M, the rest of the paper is based on this simple mask. Further results with different masks can be found in Appendix B.

It follows a closer inspection of the CNN that instantiates the reconstruction function $f_{\text{CNN}}(\cdot; \theta)$ and the architectural details of the CNN are displayed in Table I. Note that the architecture is based on convolutional layers and that fully connected layers are *avoided* in order to lower the number of training parameters. Moreover, convolutional architectures, once trained, are applicable
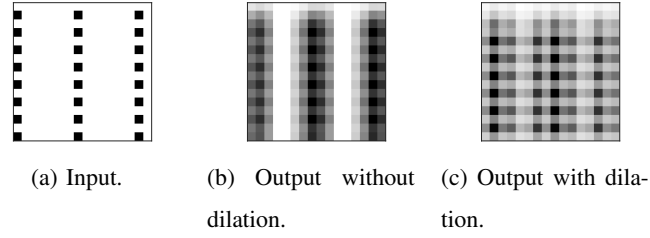
(a) Input. (b) Output without dilation. (c) Output with dilation.

Figure 4. Example of the affected output of a two layer convolutional neural network in each case with and without dilation. The "pixels" that are affected by the input are highlighted with gray levels. In both cases, the network is fed with the same binary sparse input, where the black squares represent a non-zero input value. It can be observed that using dilation larger than one in the first layer helps to progressively complete the matrix, compared to a neural network that uses standard convolutions.

to various channel dimensions as shown in [23]. In particular, here, except in the last layer, we always have convolutional layers with dilation larger then 1, cf. [24]. The advantage of using dilated convolutions for sparse inputs is illustrated in Figure 4a–4c, where the affected output in terms of matrix entries after two standard convolutional layers (Fig. 4b) is compared to the affected output obtained after two convolutional layers, where the first convolutional layer uses a dilatation of 2 (Fig. 4c). There, it can be observed that because of the dilation, the filters of the convolutional layers can be tuned in order to complete the full matrix, whereas with standard convolutions we have some residual error, since some matrix entries always remain unaffected, despite the filters we choose. One option for completing the matrix with standard convolutional layers could be to increase the number of layers itself, however, this would require different architectures for different sparsity levels.

Before feeding the input vector $\boldsymbol{h}_{\mathrm{UL}}$ in the convolutional layers, we reshape it as a sparse tensor with dimension $N_{\mathrm{a}} \times N_{\mathrm{c}} \times 2$, where the elements of $\boldsymbol{h}_{\mathrm{UL}}$ are located in the same places as the non-vanishing entries of the binary matrix $\boldsymbol{M}$. After each convolutional layer, the input tensor is gradually completed to eventually obtain $\hat{\boldsymbol{H}}_{\mathrm{UL}}^{\mathrm{real}}$. The goal of the CNN is to instantiate a function $f_{\mathrm{CNN}}(\cdot; \boldsymbol{\theta})$ which reconstructs an output $\hat{\boldsymbol{H}}_{\mathrm{UL}}^{\mathrm{real}}$ approximately equal to the original channel $\boldsymbol{H}_{\mathrm{UL}}^{\mathrm{real}}$, i.e.,

$$f_{\mathrm{CNN}}(\boldsymbol{h}_{\mathrm{UL}}; \boldsymbol{\theta}) = \hat{\boldsymbol{H}}_{\mathrm{UL}}^{\mathrm{real}} \approx \boldsymbol{H}_{\mathrm{UL}}^{\mathrm{real}},$$

where $\boldsymbol{\theta}$ refers to the adjustable weights of the CNN. To this end, the training phase of the CNN is based on a typical empirical risk function, the loss function of which is given by

$$L(\boldsymbol{\theta}, \boldsymbol{H}_{\mathrm{UL}}^{\mathrm{real}}) = \| f_{\mathrm{CNN}}(\mathrm{vec}(\boldsymbol{H}_{\mathrm{UL}}^{\mathrm{real}} \odot \boldsymbol{M}); \boldsymbol{\theta}) - \boldsymbol{H}_{\mathrm{UL}}^{\mathrm{real}} \|^2.$$
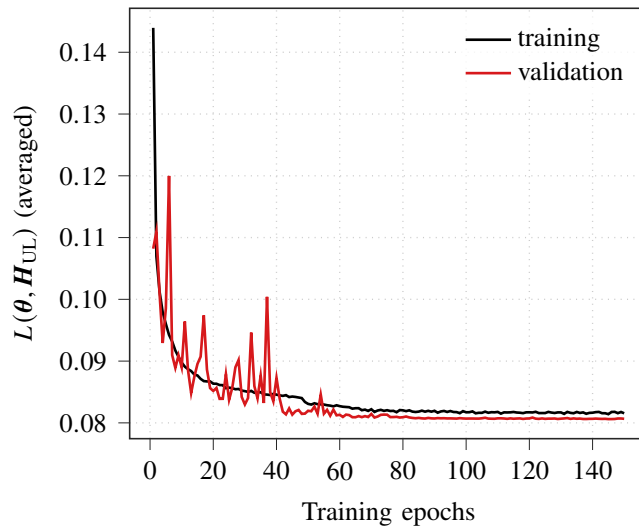
Figure 5. Evolution of training and validation loss during UL training.

IV. RETRIEVAL IN THE DOWNLINK DOMAIN

Once the parameters $\boldsymbol{\theta}$ of the CNN are learned, based only on UL data, the CNN is "transfered" to the DL frequency domain by applying it on the downsampled DL channel $\boldsymbol{h}_{\mathrm{DL}}$. In order to enable the reconstruction of the DL CSI, the downsampled DL channel $\boldsymbol{h}_{\mathrm{DL}}$ has to share the same formatting and size as $\boldsymbol{h}_{\mathrm{UL}}$ in the UL domain. Consequently, the MT has to feed back the DL coefficients to the BS according to the non-vanishing entries of the mask $\boldsymbol{M}$, i.e.,

$$\boldsymbol{h}_{\mathrm{DL}} = \mathrm{vec}(\boldsymbol{H}_{\mathrm{DL}}^{\mathrm{real}} \odot \boldsymbol{M}). \tag{5}$$

Subsequent to an equal reshaping of $\boldsymbol{h}_{\mathrm{DL}}$ as introduced in Section III for $\boldsymbol{h}_{\mathrm{UL}}$, the full DL CSI is eventually recovered by means of the trained CNN, i.e.,

$$\hat{\boldsymbol{H}}_{\mathrm{DL}}^{\mathrm{real}} = f_{\mathrm{CNN}}(\boldsymbol{h}_{\mathrm{DL}}; \boldsymbol{\theta}). \tag{6}$$

Note again, that the CNN applied to the DL data is based on the UL data.

As already mentioned before, the basis for this straightforward application of the UL-trained CNN to the fed back DL CSI is the conjecture that learning the channel recovery in the UL domain is transferable to the DL domain. In Section VII, a statistical analysis based on the maximum mean discrepancy (MMD) metric supports our argumentation.

V. Results and discussion

The CNN has been implemented with Tensorflow [25] and the training has been done with single precision numbers. We consider mini-batches of 64 samples and we use the Adam optimizer [26] to update the weights of the neural network for every batch. An epoch consists of 3750 batches and at the end of each epoch we utilize the validation set only for computing the validation loss. In Figure 5, it can be observed that 100 epochs are required to reach convergence in terms of validation loss, which corresponds to a number of batches in the order of 10^6. The typically high number of training examples in applications with CNNs poses little problem in the approach presented here, since the training data is based exclusively on UL CSI. It can be assumed that this is regularly estimated anyway during UL operation of the communication link and that a representative sampling of the propagation scenario is ensured over time due to the users being in the cell and moving around. A detailed study of such an acquisition of the radio properties of the environment is subject to further studies which are beyond the scope of this paper.

After the training, the performance is evaluated in terms of normalized mean square error ε^2 and cosine similarity ρ for the test sets with frequency gaps of $\Delta f = 120...480$ MHz, where

$$\varepsilon^2 = \mathbb{E}\left[\frac{\|\hat{\boldsymbol{H}} - \boldsymbol{H}\|_{\mathrm{F}}^2}{\|\boldsymbol{H}\|_{\mathrm{F}}^2}\right], \tag{7}$$

and

$$\rho = \mathbb{E}\left[\frac{1}{N_{\mathrm{c}}} \sum_{n=1}^{N_{\mathrm{c}}} \frac{|\hat{\boldsymbol{h}}_n^{\mathrm{H}} \boldsymbol{h}_n|}{\|\hat{\boldsymbol{h}}_n\|_2 \|\boldsymbol{h}_n\|_2}\right], \tag{8}$$

with $\boldsymbol{H} \in \mathbb{C}^{N_{\mathrm{a}} \times N_{\mathrm{c}}}$ and its n-th column $\boldsymbol{h}_n$, and $\hat{\boldsymbol{H}}$ and $\hat{\boldsymbol{h}}_n$ their corresponding reconstructed versions. The results of the performance metrics are shown in Figure 6, where for each box the median, the first quartile (Q_1) and third quartile (Q_3) are highlighted. The whiskers in the box-plots are chosen to be one and half time of the interquartile range (IQR) below the first quartile, and above the third quartile (in formulas, $Q_1 - 1.5 \times \mathrm{IQR}$ and $Q_3 + 1.5 \times \mathrm{IQR}$). Note that Q_1 represents the 25th percentile of the data, Q_3 represents the 75th percentile of the data, and IQR represents the difference between the third and the first quartile. The values outside the range covered by the whiskers are considered outliers.

In Figures 7a and 7b, the CDFs of ε^2 and ρ are additionally displayed on a logarithmic scale and compared with the retrieved DL CSI recoveries with a conventional linear interpolation of the fed back CSI in the frequency domain [27]. The latter serves as a reference in this work. It is clear from Figure 6 and Figures 7a and 7b that the CNN for DL CSI performs very well, with
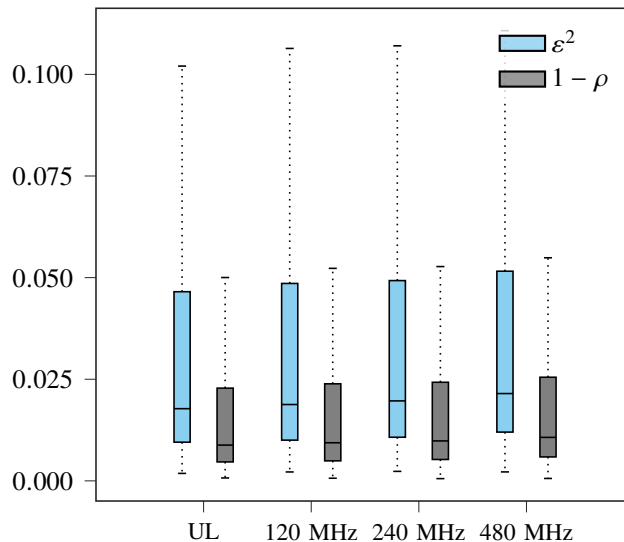
Figure 6. NMSE and cosine similarity for recovered UL CSI and DL CSI based on the same CNN and propagation scenario.

only a slight drop in performance for increasing frequency spacing, even though the CNN has never seen training samples from the downlink frequency domain and the beamsquint effect for different center frequencies has been taken into account. For all scenarios, the uplink-based CNN clearly outperforms the reference solution. For other compression ratios η the reader may refer to Appendix A to obtain a first impression. A detailed study of the appropriate compression technique and an investigation of the trade-off between compression ratios and achievable performance is considered to be subjects of future research.

A. Sum rate results and discussion

Although mean square error and cosine similarity are well-known and established performance criteria, this section additionally evaluates the quality of the channel reconstruction in a multi-user communication scenario, which in contrast to a single-user scenario is more susceptible to inaccurate CSI. In particular, we examine the quality of the channel reconstructions in terms of their achievable sum rate in a multi-user downlink scenario. To this end, the Linear Successive Allocation Algorithm (LISA) [28], [29] is applied to randomly selected test channels.[4] Each channel is associated with a channel matrix in the DL frequency domain, which is then subject to feedback and the subsequent machine learning based recovery at the BS. LISA is a zero-

---

[4]Please note that any other multi-user precoding technique can be applied as well.

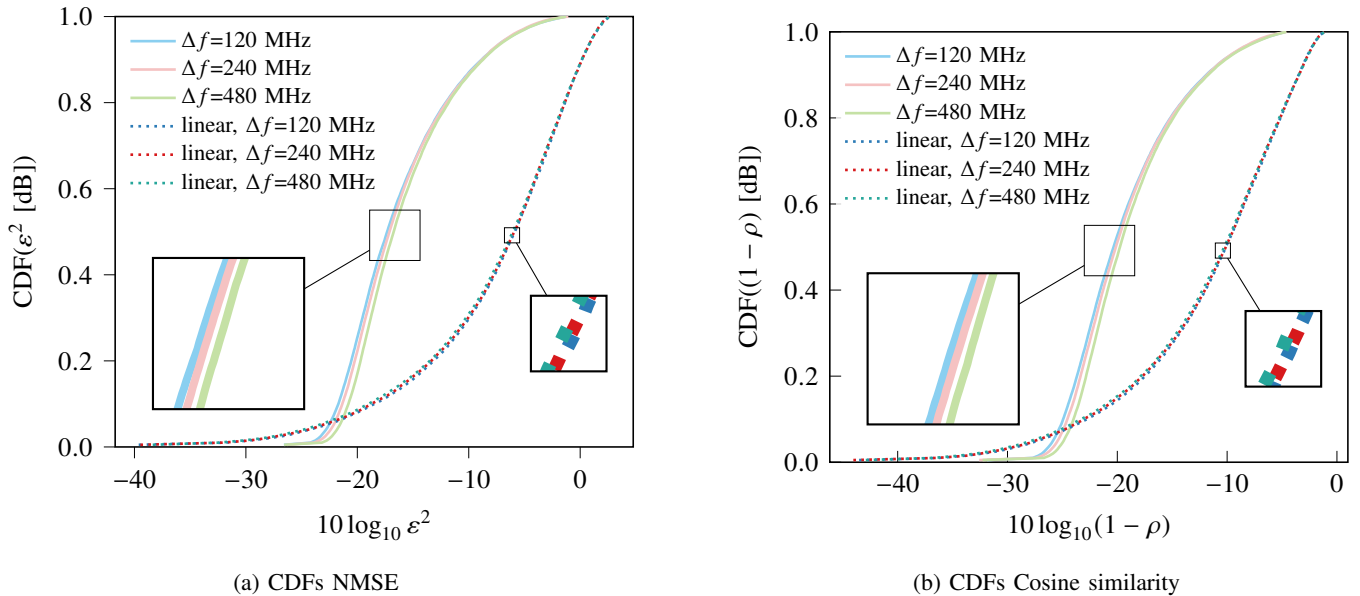(a) CDFs NMSE

(b) CDFs Cosine similarity

Figure 7. Empirical CDFs of NMSE and cosine similarity for recovered UL and DL based on the same CNN and propagation scenario.

forcing based precoding technique that simultaneously performs combined data stream and user selection, resulting in an LQ decomposition of the overall channel matrix consisting of the selected subchannels. The lower triangular matrix (L-factor) of the decomposition corresponds to the effective channel of the resulting pre-equalized system. If elaborate nonlinear coding schemes are not an option [30], a second precoding step transforms the resulting channel diagonally and results in a zero-forcing solution of the selected users. Finally, a water filling procedure is applied to the diagonal channel. For simplicity, the linear version of LISA is applied independently on each of the 160 carriers of the communication links and the results are then averaged over the carriers.

Furthermore, we considered four different scenarios with 1, 2, 4, and 8 users.

Figures 8a–8c show the average achievable per-user rate for a 120...480 MHz frequency gap over 100 instances of LISA simulation runs, respectively. The continuous lines represent the rate achievable with perfect DL CSI knowledge, the dashed lines represent the rate obtained with the DL CSI predicted with the CNN, and the dotted lines represent the rate achievable with the DL CSI as result of the linear interpolation of the DL feedback. We can observe that the achievable rate per user with the channels recovered with the CNN is close to the case of perfect CSI and that the gain of the CNN approach compared to the linear interpolation method is particularly

salient in a multi-user setup, while in single-user scenarios the linear interpolation technique is sufficient. This is due to the known lower CSI requirements in cases where preequalization of multiple channels is not required. However, the linear interpolation technique clearly fails in multi-user scenarios.

VI. APPLYING THE CNN IN UNKNOWN ENVIRONMENTS

In this section, to investigate the scenario dependency, we apply the trained CNN based on the UL CSI to the DL feedback of another cell with different properties which were unknown during the training of the CNN. In particular, we considered the urban macrocell (UMa) NLoS scenario from QuaDRiGa. The only elements in common between the cell used for the UL training and the other cell are number and the type of antennas considered at the BS and the MS, the bandwidth, and the number of carriers considered. Specifically, the number of MPCs in UMi NLoS and UMa NLoS are relatively similar (61 in UMi and 64 in UMa). However, the UMa and UMi scenarios differ not only in the number of MPCs, but in many other parameters involved in the channel realization.

The results of NMSE and the cosine similarity are shown in Figure 9. When we compare the performance metrics of the UMa NLoS cell with those of the UL baseline we can see that the CNN, which was trained on a UMi NLoS scenario does not generalize well to the UMa NLoS scenario.

This is due to the model-free learning of the CNN, which is based on the specific UL data of the cell and its propagation characteristics that is different from the data of the other cell to which the CNN is applied. However, further research, which we do not present here, has revealed that the CNN can also generalize to scenarios with similar characteristics to the scenario on which the CNN was trained, or to scenarios in which the CSI is frequency flatter. Nevertheless, the results in this section show that in principle we cannot apply the CNN trained on one propagation environment to any other arbitrary environment without extra measures. Please, note that considering changes in the environment is beyond the scope of this specific work. Regarding the actual implementation of the proposed architecture one could expect a three-phases approach similar to the one in [31] with the key-difference that in our case the training phase is *centralized* at the BS rather than *federated* over multiple devices. Moreover, since the training is carried with the sole UL data, the BS might update the weights of the CNN regularly as background activity. In this way, the algorithm can be robust to changes in the environment, also taking into

account that severe changes in the environment, as the construction of a new building, happen over a long time interval.

VII. VERIFYING THE CONJECTURE

The presented results obviously support our fundamental conjecture that learning the channel reconstruction in the UL domain can be "transfered" over the frequency gap between UL and DL center frequencies. In this section, we discuss our intuition behind this conjecture and attempt to falsify the conjecture by examining its limits of applicability.

To investigate the rationale, it is recommended to discuss in more detail the significance of the carrier frequency on the individual parameters of the channel state information. We quickly find that changing the carrier frequency primarily changes the phases of the harmonic signals carried by the corresponding propagation paths. The argumentation is now as follows. For simplicity, we assume the case of a linear uniform array and a single path propagation of a wavefront incident on the antenna array. In this case, the part of the channel vector h relevant to this discussion can be expressed by

$$h \propto [\alpha^0, \alpha^1, \alpha^2, \ldots, \alpha^{N-1}]$$

with $\alpha = \exp\left(-j\frac{2\pi df}{c}\sin\theta\right)$, where N represents the number of antenna elements, d represents the distance between the elements, f represents the carrier frequency of the transmitted narrowband signal, c represents the speed of light, and θ represents the angle of incidence of the incident wavefront on the antenna array. From this model, one can conclude that small changes δf in the carrier frequency can be compensated by small changes $\delta\theta$ of θ, i.e., the channel vector h is not changed as long as

$$f\sin\theta = (f + \delta f)\sin(\theta + \delta\theta)$$

holds. This means, at least for the special case of the assumed channel model, that from the point of view of the antenna array, for each UL channel vector of a first MT, another second MT can be assumed at a different position with a different angle of arrival of its incident wavefront, but whose DL channel vector is the same as the UL channel vector of user first MT. This is the basis of our intuition: if we observe sufficiently many constellations of channel vectors in the UL and DL domains, we will of course not observe reciprocity between the paired UL and DL vectors of any particular user. However, if we consider the aggregate of a large number of users, that could typically be recorded during standard operation of a BS to generate the training data
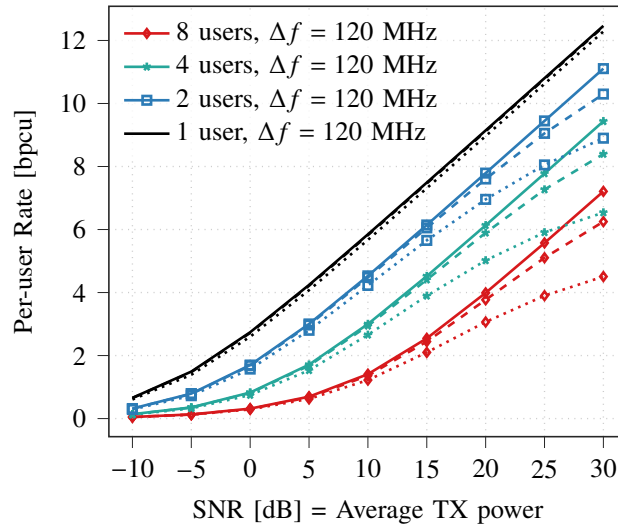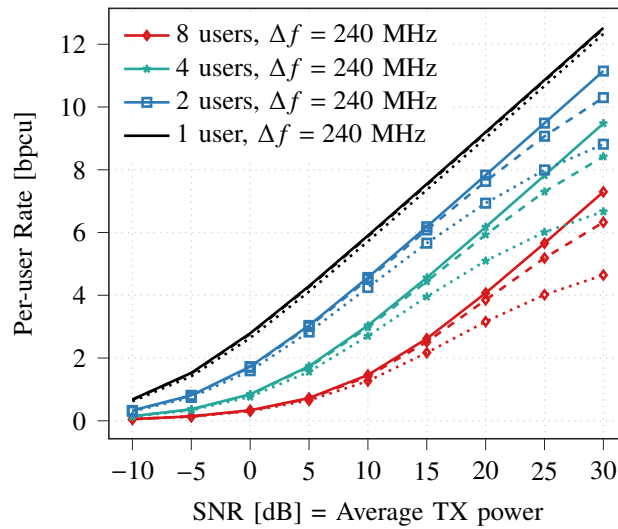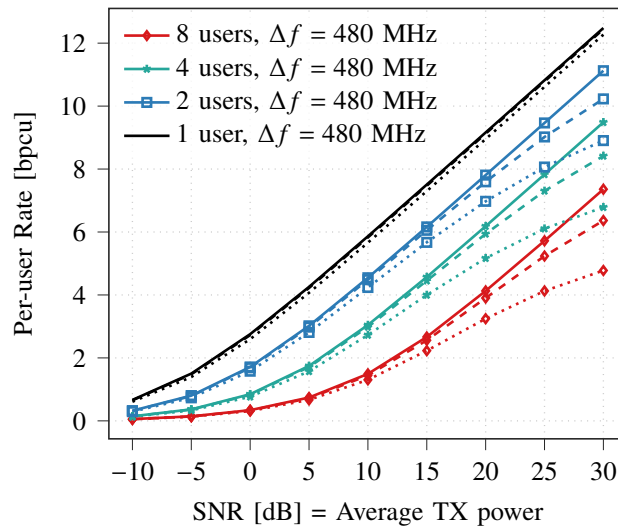
(a) $\Delta f = 120$ MHz

(b) $\Delta f = 240$ MHz

(c) $\Delta f = 480$ MHz

Figure 8. Per-user rate results with LISA for perfect (solid), recovered (dashed) and linearly interpolated (dotted) DL CSI knowledge based on fed back DL CSI with compression ratio $1/\eta = 40$.
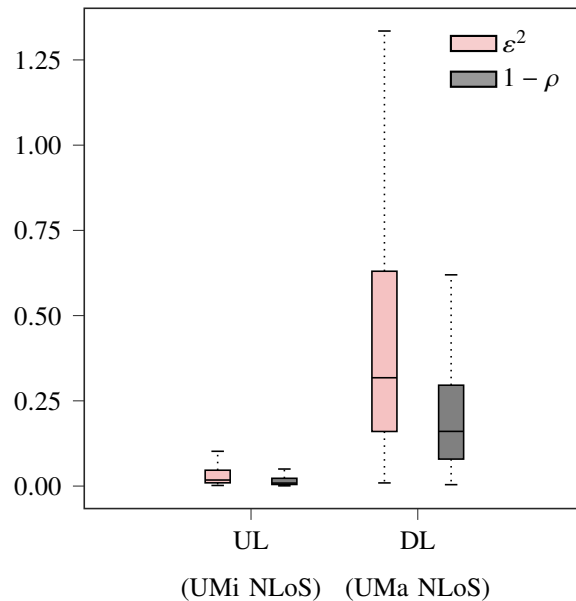
Figure 9. NMSE and cosine similarity for UL CSI versus DL CSI.

set that is needed anyway, we will still find that the distribution of the respective UL channels and the distribution of the respective DL channels are nearly equal separately from each other and only when considered by themselves.

A transfer of the above argumentation for broadband signals and channels on the basis of multipath propagation seems obvious, even if still in the status of a conjecture. This conjecture now states that the totality of all UL channels and the totality of all DL channels have approximately the same properties and can be described with the same or very similar probability distribution, even if individual UL-DL pairs are of course very different.

The authors are aware of the speculative nature of this reasoning, especially in the case of rich multipath propagation. For this reason, we move to a less qualitative and, on the other hand, more quantitative argumentation. For this purpose, we apply the maximum mean discrepancy measure (MMD) to samples of UL channels on the one hand and DL channels on the other. Along with this, we reformulate our conjecture in that we now assume that samples of UL channels and DL channels of the same scenario represent an identical or similar probability distribution of channel parameters. If this is true, it supports the explanation why a CNN learned with UL channels generalizes on DL channel data.

A. Maximum Mean Discrepancy

In this section, we introduce the kernel based definition of the so called maximum mean discrepancy (MMD) measure, see [32], [33], and [34] for more details. The MMD serves as a means to measure the discrepancy between two probability distributions purely based on its respective samples.

Definition: Given a positive definite kernel $k(\cdot, \cdot) = \langle \varphi(\cdot), \varphi(\cdot) \rangle$ of a reproducing kernel Hilbert space (RKHS) $\mathcal{H}_k$ with a feature map $\varphi(\cdot) \in \mathcal{H}_k$, the maximum mean discrepancy (MMD) between two probability distributions $\mathbb{P}$ and $\mathbb{Q}$ can be obtained by

$$\text{MMD}^2(\mathbb{P}, \mathbb{Q}, k) := \mathbb{E}[k(p, p') + k(q, q') - 2k(p, q)], \tag{9}$$

with random variables $(p, p') \sim \mathbb{P} \times \mathbb{P}$ and $(q, q') \sim \mathbb{Q} \times \mathbb{Q}$. It follows that $\text{MMD}(\mathbb{P}, \mathbb{Q}, k) = 0$ if and only if $\mathbb{P} = \mathbb{Q}$. If we further assume that we have sample sets $\mathcal{P} \sim \mathbb{P}$ and $\mathcal{Q} \sim \mathbb{Q}$ of equal sample size n, an unbiased estimator of the squared MMD for measuring the discrepancy between $\mathbb{P}$ and $\mathbb{Q}$ can be obtained by

$$\widehat{\text{MMD}}^2(\mathcal{P}, \mathcal{Q}, k) := \frac{1}{n(n-1)} \sum_{i \neq j} h_{ij}, \tag{10}$$

where $h_{ij} := k(p_i, p_j) + k(q_i, q_j) - k(p_i, q_j) - k(q_i, p_j)$ with $p_i \in \mathcal{P}$ and $q_i \in \mathcal{Q}$ being the realizations of the random variables $p \sim \mathbb{P}$ and $q \sim \mathbb{Q}$. Following the usual kernel trick, we swap the choice of feature map $\varphi(\cdot)$ with the decision for a kernel function $k(\cdot, \cdot)$. The most common choice for a kernel is the Gaussian kernel, i.e.,

$$k(p, q) = \exp\left(-\frac{\|p - q\|^2}{\sigma_{50}^2}\right),$$

where $p \in \mathcal{P}$ and $q \in \mathcal{Q}$ are two samples drawn from $\mathbb{P}$ and $\mathbb{Q}$ and σ_{50} corresponds to the 50-percentile (median) distance between elements in the aggregate sample, as suggested in [32]. To apply the MMD to the problem at hand, we compute the discrepancy between the UL CSI sample $\mathcal{P}_{\text{UL}}$ versus the DL CSI sample $\mathcal{Q}_{\text{DL}}$. In particular, we consider four different cases, i.e., the MMD of UL versus DL CSI samples in the same cell for a frequency gap of $\Delta f = 120...480$ MHz and the MMD in case of a transfer of the UL-learned CNN to an unknown different environment but for a frequency gap of only $\Delta f = 120$ MHz. Note that the environment considered here is the same as that we discussed in Section VI.

The corresponding results of the $\widehat{\text{MMD}}^2$ are shown in Figure 10, where for each test the $\widehat{\text{MMD}}^2$ has been computed for 100 paired sets $\mathcal{P}_{\text{UL}}$ and $\mathcal{Q}_{\text{DL}}$ drawn from the fixed but unknown
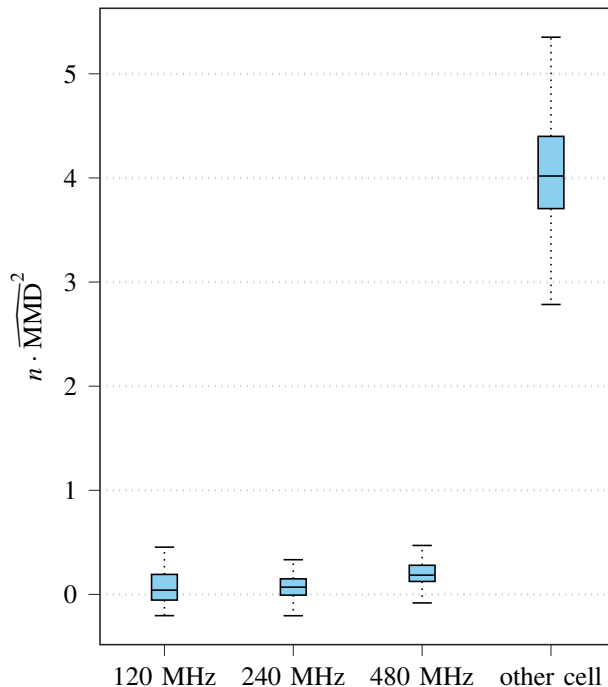
Figure 10. Empirical MMD for UL CSI versus DL CSI.

distributions $\mathbb{P}_{\text{UL}}$ and $\mathbb{Q}_{\text{DL}}$ of the uplink and downlink channel state information of the respective scenario and cell. The size of each sample is kept constant with $n = 1000$ for both $\mathcal{P}_{\text{UL}}$ and $\mathcal{Q}_{\text{DL}}$. We can observe how the MMD for channels that belong to the same cell is much smaller than the MMD between the UL of the former cell and the DL of a different cell. Moreover, for the same cell the median value of the box increases as we increase the frequency gap.

B. Hypothesis testing of the conjecture

A typical feature of the introduced MMD metric is that, being purely data-based, it is per se a random variable and thus its practical application necessarily entails hypothesis testing. As a consequence, the sole computation of a single MMD metric is not sufficient to prove our conjecture. When having a closer look at the MMD values, we see that they are rather small. Therefore, the question we address in this section is how small the $\widehat{\text{MMD}}^2$ actually needs to be to confirm the hypothesis that the two samples $\mathcal{P}_{\text{UL}}$ and $\mathcal{Q}_{DL}$ of CSI belong to the same distribution. To this end, we follow a method proposed by [34], and originally by [35] which is called a permutation test. For this purpose, let us define the null hypothesis H_0 as the hypothesis that the uplink distribution $\mathbb{P}_{\text{UL}}$ is equal to the downlink distribution $\mathbb{Q}_{\text{DL}}$, and let us denote

---

Algorithm 1 True positive rate (TPR) for H_1 of the conjecture given a false alarm rate of 5%

$t = 0$

for $i = 1 : $#iterations **do**

    $\mathcal{P}_{\mathrm{UL}} \leftarrow n$ random samples drawn from $\mathbb{P}_{\mathrm{UL}}$

    $\mathcal{Q}_{\mathrm{DL}} \leftarrow n$ random samples drawn from $\mathbb{Q}_{\mathrm{DL}}$

    $d \leftarrow \widehat{\mathrm{MMD}}^2(\mathcal{P}_{\mathrm{UL}}, \mathcal{Q}_{\mathrm{DL}}, k)$

    $\mathcal{D} = \varnothing$

    for $j = 1 : $#permutations **do**

        $\mathcal{P} \leftarrow n$ randomly selected from both $\mathcal{P}_{\mathrm{UL}}$ and $\mathcal{Q}_{\mathrm{DL}}$ without replacement

        $\mathcal{Q} \leftarrow n$ randomly selected from both $\mathcal{P}_{\mathrm{UL}}$ and $\mathcal{Q}_{\mathrm{DL}}$ without replacement

        $\mathcal{D} \leftarrow \mathcal{D} \cup \widehat{\mathrm{MMD}}^2(\mathcal{P}, \mathcal{Q}, k)$

    end for

    if $d > 95$-th percentile of $\mathcal{D}$ **then**

        $t \leftarrow t + 1$ (reject the null hypothesis)

    end if

end for

TPR $\leftarrow t/$#iterations

---

with H_1 the alternative hypothesis $\mathbb{P}_{\mathrm{UL}} \neq \mathbb{Q}_{\mathrm{DL}}$. If then H_0 is true, the samples $\mathcal{P}_{\mathrm{UL}}$ and $\mathcal{Q}_{\mathrm{DL}}$ are obviously interchangeable. To obtain a meaningful estimation of the conditional distribution of $\widehat{\mathrm{MMD}}^2$ assuming H_0 is true, the metric is then repeatedly calculated based on appropriately regenerated data sets $\mathcal{P}$ and $\mathcal{Q}$. These data sets are constructed by uniformly resampling the union of the original data sets $\mathcal{P}_{\mathrm{UL}} \cup \mathcal{Q}_{\mathrm{DL}}$ without replacement, which can also be viewed as splitting the union of the original data sets into two equal sets subsequent to a random permutation. Once a sufficiently large sample of the conditional distribution of the random variable $\widehat{\mathrm{MMD}}^2$ is derived, a false alarm rate for the alternative hypothesis can be introduced and the corresponding decision threshold of the hypothesis test be derived. In contrast, sampling $\widehat{\mathrm{MMD}}^2$ assuming H_1 is true cannot be based on resampling or splitting the union of the two data sets under test, but requires multiple original datasets of CSI from the UL and DL domains. The main principle of this method is outlined in the Algorithm 1.

Finally, evaluating the true positive rate of H_1 provides a suitable basis to conclude whether
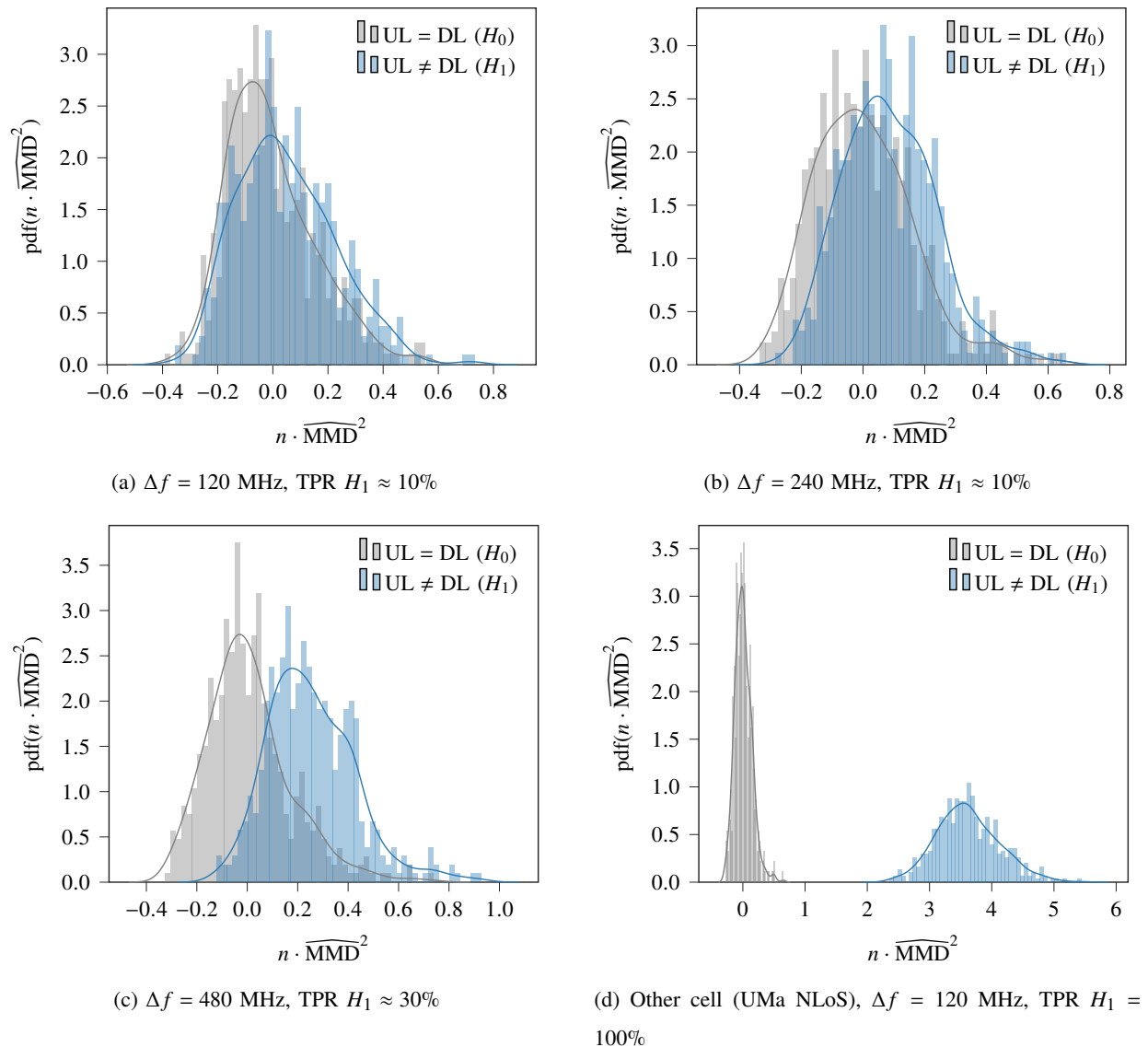
(a) $\Delta f = 120$ MHz, TPR $H_1 \approx 10\%$

(b) $\Delta f = 240$ MHz, TPR $H_1 \approx 10\%$

(c) $\Delta f = 480$ MHz, TPR $H_1 \approx 30\%$

(d) Other cell (UMa NLoS), $\Delta f = 120$ MHz, TPR $H_1 = 100\%$

Figure 11. Empirical MMD distributions assuming H_0 or H_1 is true, and corresponding TPR for a false alarm rate of 5%.

the distributions of CSI at UL and DL frequencies are the same. In Figures 11a–11d, we show the empirical distribution of the $\widehat{\text{MMD}}^2$ for both the two hypothesis H_0 and H_1. In order to define the hypothesis test for a each pair of UL and DL samples $\mathcal{P}_{\text{UL}}$ and $\mathcal{Q}_{\text{DL}}$, each of sample size $n = 1000$, we generate 500 realizations of $\widehat{\text{MMD}}^2$ assuming H_0 is true (#permutations) by the respective generation of paired samples $\mathcal{P}$ and $\mathcal{Q}$. The determination of the true positive rate (TPR) of the hypothesis test is then based on 100 test runs (#iterations) and thus on the corresponding equal number of paired samples $\mathcal{P}_{\text{UL}}$ and $\mathcal{Q}_{\text{DL}}$, cf. Algorithm 1. Each test is designed with respect to a false alarm rate of 5%. The resulting TPR is equal with the number

of test runs where the MMD indicates a discrepancy between $\mathcal{P}_{\mathrm{UL}}$ and $\mathcal{Q}_{\mathrm{DL}}$ over the total number of tests.

The obtained results validate our conjecture and confirm that when we have a small gap we can utilize uplink data for training instead of downlink data. Moreover, in Figure 11d we can clearly see the asymptotic behavior of the $\widehat{\mathrm{MMD}}^2$ which has been outlined in [32]. Therein, it is reported that the null hypothesis H_0 is distributed as an infinite-χ^2-sum, while the alternative hypothesis H_1 is normal distributed. For more details, please refer to [32]. It should also be mentioned, that the obtained values of $\widehat{\mathrm{MMD}}^2$ depend on the choice of the applied kernel. Consequently, in future work, the analysis of the conjecture could be extended to multiple kernels to eliminate a possible bias of a chosen kernel. On the other hand, due to the universality of the Gaussian kernel, the results obtained are certainly of sufficient quality for the investigations carried out in this work.

VIII. Conclusion

In this work, we have addressed the problem of channel acquisition for the downlink in FDD communication systems, which typically suffers from the fact that the required CSI cannot be estimated directly at the BS. The classical method for solving this problem is to report back to the base station the channel itself, properties of the channel or quality characteristics derived from it. This work also follows such a general feedback concept by reporting a considerably compressed channel state information to the BS, which subsequently reconstructs the full downlink CSI based on the received feedback. Our novel contribution is that we perform this channel reconstruction using a convolutional neural network and, based on the essential assumption that the CNN can be trained solely on the basis of collected uplink CSI, that the supervisory learning of the CNN is performed without providing downlink data, thus, saving a huge signaling overhead throughout the communication system. On the contrary, it may be assumed that the required training data for purely uplink-based learning is generated anyway during standard uplink operation of the communication link, and thus the provision of the training data does not involve any extra effort. It has been shown that the proposed method clearly outperforms a linear interpolation scheme in terms of conventional performance metrics. When applying the reconstructed downlink CSI for downlink precoding in a multi-user MIMO communication scenario, it even comes close to the performance achieved when assuming the full knowledge of the downlink CSI at the BS. The second part of this paper was devoted to strengthening the aforementioned "transfer learning"
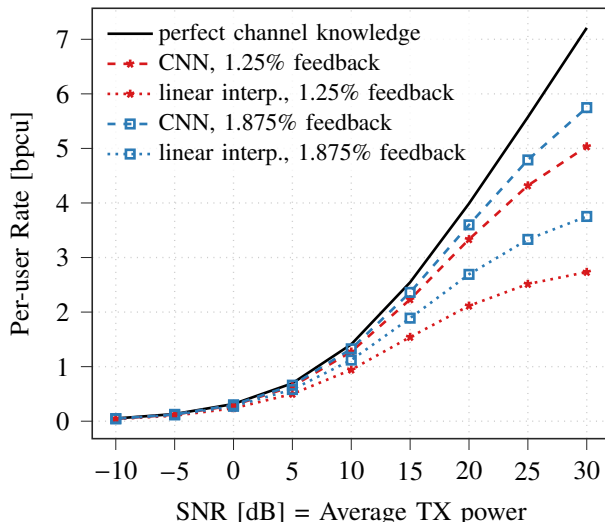
Figure 12. Per-user rate results with LISA in a multiuser scenario with 8 users with compression ratios $1/\eta \approx 54$ and $1/\eta = 80$.

conjecture we have raised by analyzing the equivalence of uplink and downlink CSI for the purpose of learning the weights of the CNN.

It is left to future research to further analyze suitable compression schemes of downlink CSI for the intended purpose, the effect of inaccurate channel estimation at the mobile terminal or possible quantization effects. We also intend to address the consideration of the inevitable outdating of the CSI and how it can be accounted for in the learning scheme.

APPENDIX A
LARGER COMPRESSION RATIOS

In this section, we investigate the performance degradation when using smaller quantities of feedback. In particular, we consider the feedback quantities of 1.25% and 1.875%.

Once again, the average results of NMSE and cosine similarity for 1.25% and 1.875%, which for the sake of brevity we do not report here, have shown that the performance of the DL CSI are extremely similar to those of the UL test set, although the CNN has been trained with the sole UL CSI.

On the contrary, it might be more interesting for the reader to observe the results in terms of per-user rate in a multi-user scenario with 8 users with the two compression ratios, which are illustrated in Figure 12. In particular, we can notice that with both configurations we always improve the linear interpolation scheme. Note that, in order to slightly improve the results for

the 1.25% feedback case we have changed the values of the dilation of the CNN in Table I, from $[15, 7, 4, 2, 2]$ to $[30, 15, 7, 4, 2]$.

APPENDIX B
MASK OPTIMIZATION

In this Section, we consider the design of the mask $\boldsymbol{M}$ which has been introduced in Section III. To this purpose we decided to utilize the architecture in [36] called concrete autoencoder (CAE). The CAE has been applied to a communication problem in [37], where it has been used to find the most informative locations for pilot transmission in OFDM systems. Another very promising study was presented in the aforementioned paper by Mashhadi [20]. However, for the initial investigation of this perspective in our work, we have limited ourselves to performing the optimization of the mask $\boldsymbol{M}$ using the method in [36], since it provides an easier integration into our framework.

In the following, we first summarize the CAE framework, and then we analyze the simulation results.

A. Concrete Autoencoder

The CAE is an autoencoder where the first layer called concrete selector layer extracts the k most informative feature of the input $\boldsymbol{x} \in \mathbb{R}^d$, where $d \gg k$. Each of the k output neurons is connected to all the input features, through the weights $\boldsymbol{m}^{(i)} \in \mathbb{R}^d$, for $i = 1, \ldots k$:

$$\boldsymbol{m}_j^{(i)} = \frac{\exp\left(\log \boldsymbol{\alpha}_j + \boldsymbol{g}_j\right)/T}{\sum_{\ell=1}^{d} \exp\left(\log \boldsymbol{\alpha}_\ell + \boldsymbol{g}_\ell\right)/T}, \tag{11}$$

where $\boldsymbol{m}_j^{(i)}$ refers to the j-th element in of the vector $\boldsymbol{m}^{(i)}$, $\boldsymbol{g}$ is d-dimensional vector sampled from a Gumbel distribution [38], $\boldsymbol{\alpha} \in \mathbb{R}_{>0}^d$, and the temperature parameter $T \in (0, \infty)$. During the training of the CAE, when $T \to 0$ and $\boldsymbol{\alpha}$ becomes more sparse, the concrete random variable $\boldsymbol{m}^{(i)}$ smoothly approaches the discrete distribution, and outputs a one hot vectors with $\boldsymbol{m}_j^{(i)} = 1$ with probability $\boldsymbol{\alpha}_j / \sum_\ell \boldsymbol{\alpha}_\ell$.

B. Simulation results

The simulation results obtained with different masks are shown in Figure 13 in terms of NMSE. First of all, one can observe once again that the performances of the UL-trained neural network on DL test data is very close to the performances obtained with UL test data from the same
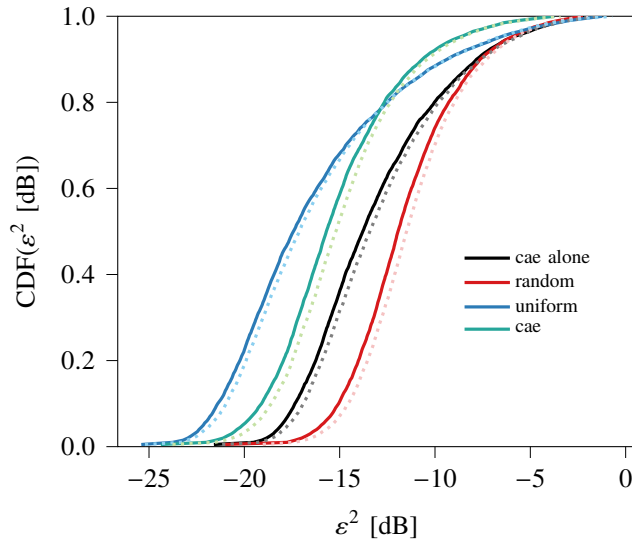
Figure 13. Empirical CDFs of NMSE for fully recovered CSI based on different masks applied to UL test data (solid) and DL test data (dotted).

distribution which the recovery network has been trained on. The black lines show the performance obtained when the CAE is trained alone without using the proposed CNN, as in [36]. The uniform mask together with the CNN which has been discussed in the previous sections outperforms the NMSE that can be obtained by training the CNN with the mask obtained after training the CAE alone. However, the average value of the NMSE obtained with the CNN trained with respect to the CAE mask (0.045 for "`cae`") is better than the average value of the NMSE obtained with the CNN trained with uniform mask (0.054 for "`uniform`"). This can be expected when having a closer look at Figure 13: approximately at the value of -13 dB the green curves are above the blue ones. Finally, all these approaches do better than the case in which the CNN is applied to a random mask.

REFERENCES

[1] T. L. Marzetta, "Noncooperative Cellular Wireless with Unlimited Numbers of Base Station Antennas," *IEEE Transactions on Wireless Communications*, vol. 9, no. 11, pp. 3590–3600, 2010.

[2] L. Sanguinetti, E. Björnson, and J. Hoydis, "Toward Massive MIMO 2.0: Understanding Spatial Correlation, Interference Suppression, and Pilot Contamination," *IEEE Transactions on Communications*, vol. 68, no. 1, pp. 232–257, 2020.

[3] E. Björnson, L. Sanguinetti, H. Wymeersch, J. Hoydis, and T. L. Marzetta, "Massive MIMO is a reality–What is next? five promising research directions for antenna arrays," *Digital Signal Processing*, vol. 94, pp. 3 – 20, 2019, special Issue on Source Localization in Massive MIMO.

[4] M. Barzegar Khalilsarai, S. Haghighatshoar, X. Yi, and G. Caire, "FDD massive MIMO via UL/DL channel covariance extrapolation and active channel sparsification," *IEEE Transactions on Wireless Communications*, vol. 18, no. 1, pp. 121–135, 2019.

[5] W. Utschick and J. A. Nossek, "Downlink beamforming for FDD mobile radio systems based on spatial covariances," in *Proceedings of the European Wireless 99 & ITG Mobile Communications*, Munich, Germany, 1999, pp. 65–67.

[6] M. Arnold, S. Dörner, S. Cammerer, S. Yan, J. Hoydis, and S. ten Brink, "Enabling FDD massive MIMO through deep learning-based channel prediction," *CoRR*, vol. abs/1901.03664, 2019.

[7] M. Alrabeiah and A. Alkhateeb, "Deep Learning for TDD and FDD Massive MIMO: Mapping Channels in Space and Frequency," in *2019 53rd Asilomar Conference on Signals, Systems, and Computers*, 2019, pp. 1465–1470.

[8] J. Wang, Y. Ding, S. Bian, Y. Peng, M. Liu, and G. Gui, "UL-CSI data driven deep learning for predicting DL-CSI in cellular FDD systems," *IEEE Access*, vol. 7, pp. 96 105–96 112, 2019.

[9] Y. Han, M. Li, S. Jin, C. K. Wen, and X. Ma, "Deep Learning-Based FDD Non-Stationary Massive MIMO Downlink Channel Reconstruction," *IEEE Journal on Selected Areas in Communications*, vol. 38, no. 9, pp. 1980–1993, 2020.

[10] M. S. Safari, V. Pourahmadi, and S. Sodagari, "Deep UL2DL: Data-Driven Channel Knowledge Transfer From Uplink to Downlink," *IEEE Open Journal of Vehicular Technology*, vol. 1, pp. 29–44, 2020.

[11] V. Rizzello, I. Brayek, M. Joham, and W. Utschick, "Learning the Channel State Information Across the Frequency Division Gap in Wireless Communications," in *WSA 2020; 24th International ITG Workshop on Smart Antennas*, 2020, pp. 1–6.

[12] D. J. Love, R. W. Heath, V. K. N. Lau, D. Gesbert, B. D. Rao, and M. Andrews, "An overview of limited feedback in wireless communication systems," *IEEE Journal on Selected Areas in Communications*, vol. 26, no. 8, pp. 1341–1365, 2008.

[13] C. Wen, W. Shih, and S. Jin, "Deep learning for massive MIMO CSI feedback," *IEEE Wireless Communications Letters*, vol. 7, no. 5, pp. 748–751, 2018.

[14] Z. Liu, L. Zhang, and Z. Ding, "Exploiting bi-directional channel reciprocity in deep learning for low rate massive MIMO CSI feedback," *IEEE Wireless Communications Letters*, vol. 8, no. 3, pp. 889–892, 2019.

[15] ——, "An efficient deep learning framework for low rate massive MIMO CSI reporting," *IEEE Transactions on Communications*, vol. 68, no. 8, pp. 4761–4772, 2020.

[16] J. Guo, C. Wen, S. Jin, and G. Y. Li, "Convolutional neural network-based multiple-rate compressive sensing for massive MIMO CSI feedback: Design, simulation, and analysis," *IEEE Transactions on Wireless Communications*, vol. 19, no. 4, pp. 2827–2840, 2020.

[17] J. Guo, C. K. Wen, and S. Jin, "Deep learning-based CSI feedback for beamforming in single- and multi-cell massive MIMO systems," *IEEE Journal on Selected Areas in Communications*, pp. 1–1, 2020.

[18] F. Sohrabi, K. M. Attiah, and W. Yu, "Deep learning for distributed channel feedback and multiuser precoding in FDD massive MIMO," *IEEE Transactions on Wireless Communications*, pp. 1–1, 2021.

[19] P. Liang, J. Fan, W. Shen, Z. Qin, and G. Y. Li, "Deep learning and compressive sensing-based csi feedback in fdd massive mimo systems," *IEEE Transactions on Vehicular Technology*, vol. 69, no. 8, pp. 9217–9222, 2020.

[20] M. B. Mashhadi and D. Gunduz, "Pruning the Pilots: Deep Learning-Based Pilot Design and Channel Estimation for MIMO-OFDM Systems," *IEEE Transactions on Wireless Communications*, vol. 1276, no. c, pp. 1–12, 2021.

[21] S. Jaeckel, L. Raschkowski, F. Burkhardt, and L. Thiele, "Efficient Sum-of-Sinusoids-Based Spatial Consistency for the 3GPP New-Radio Channel Model," in *2018 IEEE Globecom Workshops (GC Wkshps)*, 2018, pp. 1–7.

[22] M. Kurras, S. Dai, S. Jaeckel, and L. Thiele, "Evaluation of the Spatial Consistency Feature in the 3GPP Geometry-Based Stochastic Channel Model," in *2019 IEEE Wireless Communications and Networking Conference (WCNC)*, 2019, pp. 1–6.

[23] M. B. Mashhadi, Q. Yang, and D. Gunduz, "Distributed Deep Convolutional Compression for Massive MIMO CSI Feedback," *IEEE Transactions on Wireless Communications*, vol. 20, no. 4, pp. 2621–2633, 2021.

[24] F. Yu and V. Koltun, "Multi-scale context aggregation by dilated convolutions," in *4th International Conference on Learning Representations, ICLR 2016, San Juan, Puerto Rico, May 2-4, 2016, Conference Track Proceedings*, Y. Bengio and Y. LeCun, Eds., 2016.

[25] "TensorFlow: Large-scale machine learning on heterogeneous systems," 2015, software available from tensorflow.org.

[26] D. P. Kingma and J. Ba, "Adam: A Method for Stochastic Optimization," in *3rd International Conference on Learning Representations, ICLR 2015, San Diego, CA, USA, May 7-9, 2015, Conference Track Proceedings*, Y. Bengio and Y. LeCun, Eds., 2015.

[27] S. Coleri, M. Ergen, A. Puri, and A. Bahai, "Channel estimation techniques based on pilot arrangement in OFDM systems," *IEEE Transactions on Broadcasting*, vol. 48, no. 3, pp. 223–229, 2002.

[28] C. Guthy, W. Utschick, and G. Dietl, "Low complexity linear zero-forcing for the MIMO broadcast channel," *IEEE Journal on Selected Topics in Signal Processing*, vol. 3, no. 6, pp. 1106–1117, December 2009.

[29] W. Utschick, C. Stöckle, M. Joham, and J. Luo, "Hybrid LISA Precoding for Multiuser Millimeter-Wave Communications," *IEEE Transactions on Wireless Communications*, vol. 17, no. 2, pp. 752–765, 2018.

[30] P. Tejera, W. Utschick, G. Bauch, and J. A. Nossek, "Subchannel Allocation in Multiuser Multiple-Input-Multiple-Output Systems," *IEEE Transactions on Information Theory*, vol. 52, no. 10, pp. 4721–4733, 2006.

[31] M. B. Mashhadi, M. Jankowski, T. Tung, S. Kobus, and D. Gündüz, "Federated mmwave beam selection utilizing LIDAR data," *CoRR*, vol. abs/2102.02802, 2021.

[32] A. Gretton, K. M. Borgwardt, M. J. Rasch, B. Schölkopf, and A. J. Smola, "A Kernel Two-Sample Test," *J. Mach. Learn. Res.*, vol. 13, pp. 723–773, 2012.

[33] F. Liu, W. Xu, J. Lu, G. Zhang, A. Gretton, and D. J. Sutherland, "Learning Deep Kernels for Non-Parametric Two-Sample Tests," in *Proceedings of the 37th International Conference on Machine Learning, ICML 2020, 13-18 July 2020, Virtual Event*, ser. Proceedings of Machine Learning Research, vol. 119.   PMLR, 2020, pp. 6316–6326.

[34] D. J. Sutherland, H. Tung, H. Strathmann, S. De, A. Ramdas, A. J. Smola, and A. Gretton, "Generative Models and Model Criticism via Optimized Maximum Mean Discrepancy," in *5th International Conference on Learning Representations, ICLR 2017, Toulon, France, April 24-26, 2017, Conference Track Proceedings*.   OpenReview.net, 2017.

[35] M. Dwass, "Modified randomization tests for nonparametric hypotheses," *The Annals of Mathematical Statistics*, vol. 28, no. 1, pp. 181–187, 1957.

[36] M. F. Balin, A. Abid, and J. Y. Zou, "Concrete autoencoders: Differentiable feature selection and reconstruction," in *Proceedings of the 36th International Conference on Machine Learning, ICML 2019, 9-15 June 2019, Long Beach, California, USA*, ser. Proceedings of Machine Learning Research, K. Chaudhuri and R. Salakhutdinov, Eds., vol. 97. PMLR, 2019, pp. 444–453.

[37] M. Soltani, V. Pourahmadi, and H. Sheikhzadeh, "Pilot pattern design for deep learning-based channel estimation in OFDM systems," *IEEE Wirel. Commun. Lett.*, vol. 9, no. 12, pp. 2173–2176, 2020.

[38] E. J. Gumbel, *Statistical theory of extreme values and some practical applications; a series of lectures*, ser. Applied mathematics series ; 33.   Washington: U.S. Govt. Print. Office, 1954.